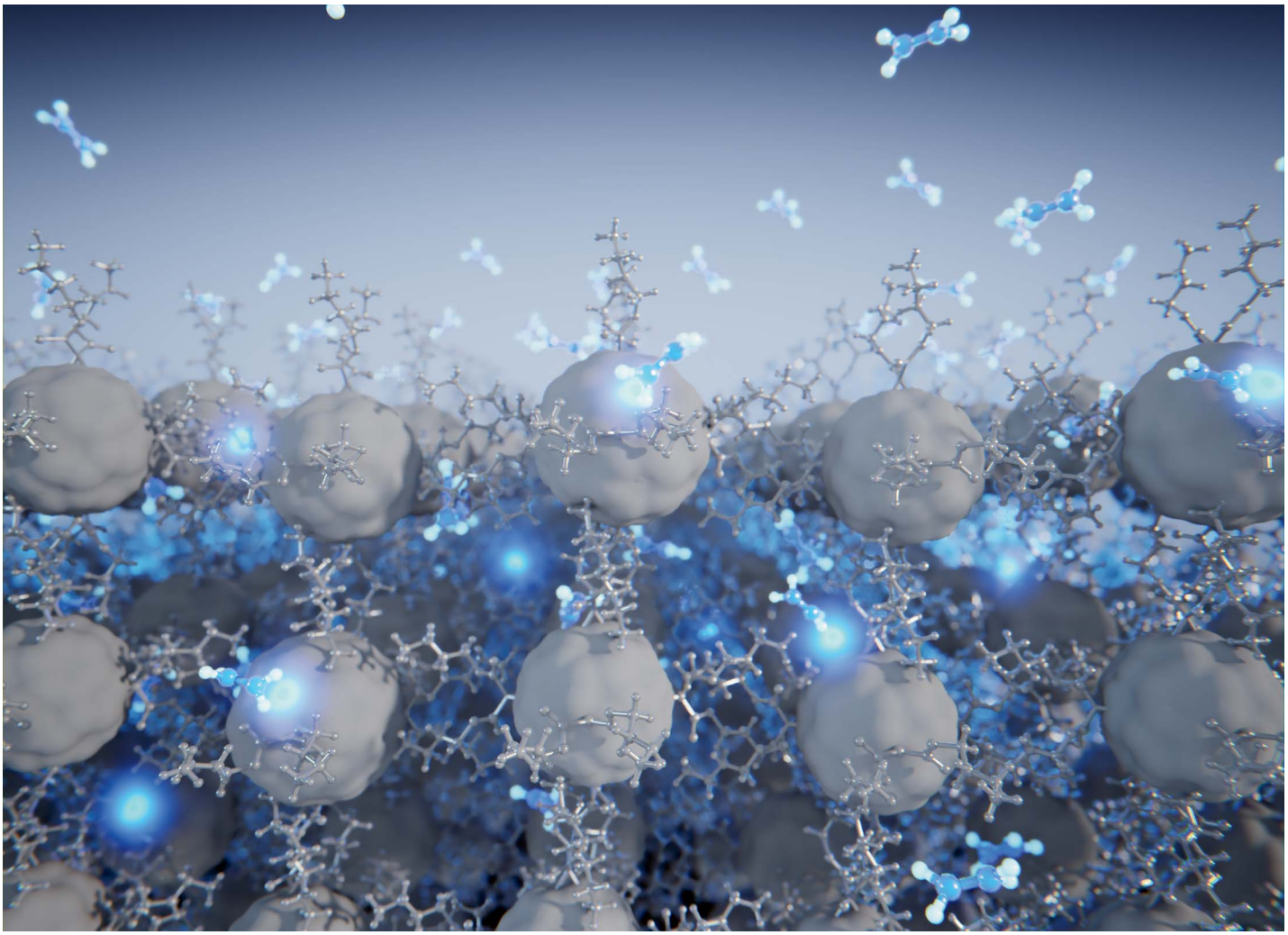

Showcasing research from Nazario Martín and José Sánchez Costa, IMDEA Nanociencia and Universidad Complutense, Madrid, Spain.

Playing with the weakest supramolecular interactions in a 3D crystalline hexakis[60]fullerene induces control over hydrogenation selectivity

Weak forces play an essential role in chemical reactions. Controlling these by applying external stimuli represents a target in supramolecular chemistry. Here, a controlled reorganization of a fullerene-based compound purely governed by the weakest van der Waals interactions, i.e. the dihydrogen interaction is illustrated. This reorganization, monitored by single-crystal to single-crystal diffraction, under mild conditions allows a selective hydrogenation via hydrazine vapor exposure.

As featured in:

See Nazario Martín, José Sánchez Costa *et al.*, *Chem. Sci.*, 2021, **12**, 8682.

ROYAL SOCIETY OF CHEMISTRY

rsc.li/chemical-science

Registered charity number: 207890

Chemical Science

ROYAL SOCIETY OF CHEMISTRY

EDGE ARTICLE

View Article Online
View Journal | View Issue

Cite this: *Chem. Sci.*, 2021, **12**, 8682

All publication charges for this article have been paid for by the Royal Society of Chemistry

Received 18th February 2021
Accepted 17th May 2021

DOI: 10.1039/d1sc00981h

rsc.li/chemical-science

Playing with the weakest supramolecular interactions in a 3D crystalline hexakis[60]fullerene induces control over hydrogenation selectivity†

Estefania Fernandez-Bartolome,[a] Arturo Gamonal,[a] José Santos,[ab] Saeed Khodabakhshi,[a] Eider Rodríguez-Sánchez,[a] E. Carolina Sañudo,[cd] Nazario Martín *[ab] and José Sánchez Costa *[a]

Weak forces can play an essential role in chemical reactions. Controlling such subtle forces in reorganization processes by applying thermal or chemical stimuli represents a novel synthetic strategy and one of the main targets in supramolecular chemistry. Actually, to separate the different supramolecular contributions to the stability of the 3D assemblies is still a major challenge. Therefore, a clear differentiation of these contributions would help in understanding the intrinsic nature as well as the chemical reactivity of supramolecular ensembles. In the present work, a controlled reorganization of an hexakis[60]fullerene-based molecular compound purely governed by the weakest van der Waals interactions known, *i.e.* the dihydrogen interaction – usually called sticky fingers – is illustrated. This pre-reorganization of the hexakis[60]fullerene under mild conditions allows a further selective hydrogenation of the crystalline material *via* hydrazine vapors exposure. This unique two-step transformation process is monitored by single-crystal to single-crystal diffraction (SCSC) which allows the direct observation of the molecular movements in the lattice and the subsequent solid–gas hydrogenation reaction.

Introduction

Weak forces are essential in a wide variety of chemical reactions. These interactions, including hydrogen bonds, π–π stacking, hydrophobic associations, electrostatic interactions and van der Waals (vdW) forces, are at the foundation of the supramolecular interactions.[1,2] Although workers in protein science, in supramolecular and theoretical chemistry have readily embraced the significance of dispersion forces,[3–5] most synthetic molecular chemists have neglected the importance of these attractive forces. Definitely, weak forces can considerably influence stability, structure and reactivity during the chemical reaction. As an example, they are responsible for the three-dimensional spontaneous, self-assembly of protein chains and the reversibility of this process under thermal or chemical treatment (folding and unfolding processes).[6,7] Controlling such subtle reorganization by applying thermal or chemical stimuli is likely one of the main targets in supramolecular chemistry.[8] A remarkable approach is the so-called topochemistry, in which the term "topochemical control" describes processes in which molecules are suitably arranged for diffusionless reactions, thus requiring the smallest atom displacement of the substrate.[9] Gaining control over these subtle reorganizations has demonstrated its relevance as a novel synthetic strategy. However, it is still very difficult to separate the different supramolecular contributions to the stability of the assemblies. The clear differentiation of these contributions would help in understanding the intrinsic nature of supramolecular assemblies.[10] Therefore, the assembly of supramolecular networks being merely dependent on one type of noncovalent interactions is very meaningful. In the present work, a controlled reorganization of a [60]fullerene-based molecular compound purely governed by the weakest van der Waals interaction known, *i.e.* the dihydrogen interaction, usually called sticky fingers, is illustrated.[11]

Fullerene C_{60} has been extensively studied since its discovery in 1985, due to its singular geometrical, redox and optoelectronic properties.[12] Among these properties, its usefulness as a building-block for obtaining octahedral geometry adducts, namely the hexakis-substituted C_{60} adducts is at the forefront (Fig. 1). Their T_h octahedral symmetry provides a unique and

[a]*IMDEA Nanociencia, Ciudad Universitaria deCantoblanco, C/ Faraday 9, Madrid, 28049, Spain. E-mail: jose.sanchezcosta@imdea.org; nazmar@quim.ucm.es*

[b]*Departamento de Química Orgánica, Facultad de Ciencias Químicas, Universidad Complutense, 28040 Madrid, Spain*

[c]*Institut de Nanociència i Nanotecnologia, Universitat de Barcelona, 08028 Barcelona, Spain*

[d]*Departament de Química Inorgànica i Orgànica, Secció química Inorgànica, Universidad de Barcelona, C/Martí i Franqués 1-11, Barcelona, 08028, Spain*

† Electronic supplementary information (ESI) available: Crystallographic details, tables of crystal and refinement data, experimental procedures and characterization for **2** and **2hyd**, and Fig. S1–S14. CCDC 2049752 and 2049753. For ESI and crystallographic data in CIF or other electronic format see DOI: 10.1039/d1sc00981h

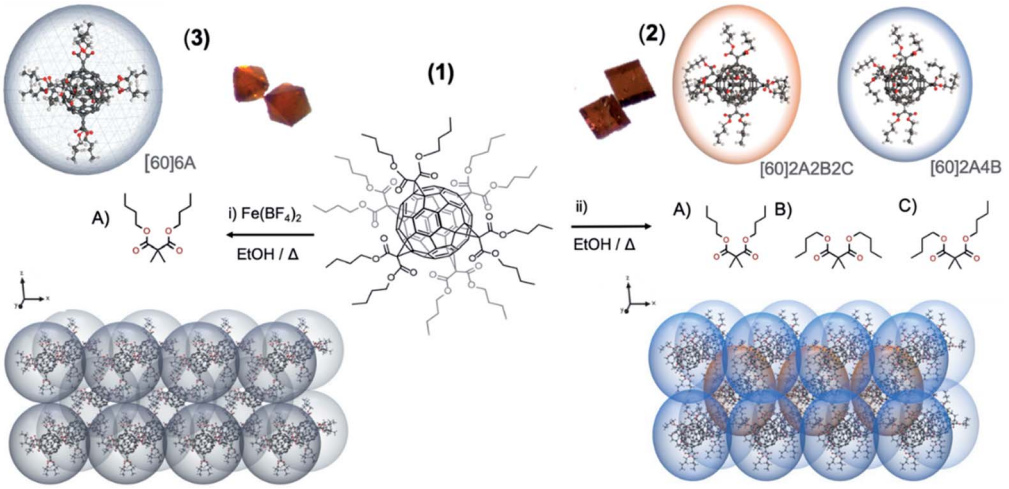

Fig. 1 Crystallization scheme for orange single crystals of **1** to achieve crystalline polymorphs **2** and **3**. The supramolecular packing of **2** is based on a single malonate-based arm conformation, whereas **3** shows three conformations, named *A*, *B* and *C*. The conformation differences give rise to an altered packing form in **2** and **3**, which could be summarized as sphere *vs.* oval shape.

attractive spherical scaffold (cage structure) which has been applied for biomedical purposes (for instance inhibiting the infection of emergent viruses[13]) as well as for the construction of multifunctional nanomaterials by self-assembly, either with itself or through metal centers.[14–21] Our research group has recently reported the first example of a van der Waals "sticky fingers" crystalline structure of a C_{60} hexakis-adduct (herein after referred as **3**).[22] The sum of several dihydrogen vdW interactions between interdigitated butyl malonate units attached to neighboring [60]fullerenes has been revealed as the driving force for the crystallization of a robust, purely molecular, dynamic framework of hexakis[60]fullerene adducts. This framework provides the excellent scaffolding for testing a new topochemical solid–vapor reaction.

Our work here shows how by exclusively controlling the dihydrogen interactions, we can pre-reorganize a hexakis[60]fullerene under mild conditions to later selectively hydrogenate the structure by exposing the crystalline material to hydrazine vapors. This unique two-step transformation process is monitored by single-crystal to single-crystal diffraction (SCSC) which allows the direct observation of the molecular movements in the lattice and the subsequent solid–gas hydrogenation reaction.

Results and discussion

The butyl-malonate hexakis[60]fullerene (**1**) has been synthesized in a straightforward method by Bingel–Hirsch cyclopropanation reaction following a previously reported methodology.[23] Crystallization of **1** from ethanol allows obtaining two well differentiated crystal structures depending on the additives employed: (i) addition of an iron salt, $[Fe(BF_4)_2]$ and (ii) metal-free solution (see ESI† for further information). Each methodology affords well differentiated either cubic (**2**) or octahedral (**3**) orange crystals, both suitable for X-ray diffraction analysis (see Fig. 1 and 4).

Structural description

Polymorph **2** crystallizes in the triclinic space group $P\bar{1}$ (see Table S1† for further details). The unit cell is composed by a total of nine fullerenes, with an hexakis[60]fullerene placed on each vertex of the polyhedron, shared by eight adjacent unit cells and one fullerene in the middle of the cube. This arrangement gives rise to a total of two non-equivalent fullerenes per unit cell distributed in three different layers. These two fullerenes are dissimilar considering the different conformations adopted by their butyl chains, as appreciated in Fig. 1 and 4. Owing to the flexible nature of butyl chains, each dibutyl malonate may exhibit three different conformations: one with both butyl chains fully extended, another with both folded, and the last one with one butyl fully extended the other folded, (named as *A*, *B* and *C* conformations, respectively). Precisely, the fullerene placed on a vertex of the unit cell has two extended butyl malonate functionalities in axial position (*A* conformation, Fig. 1), while the four malonates in equatorial display a folded conformation of their butyl chains (*B* conformation, Fig. 1). In contrast, the fullerene placed inside the unit cell shows all three possible conformations, *i.e.* axial malonates always displaying fully stretched conformation, and equatorial ones showcasing two as fully folded and two in intermediate conformations, with one butyl folded and the other stretched (Fig. 1, *A*, *B* and *C* conformations respectively). In each case, the shortest distance between two neighboring fullerenes of adjacent layers in **2** is 6.874 Å, which is out of the range for the supramolecular π–π interactions of pristine [60]fullerene.[24]

Thus, dihydrogen interactions between adjacent alkyl branches can be considered as the main driving force for the packing in **2**.

On the other hand, polymorph **3** (ref. 22) crystallizes in a different space group from **2**, namely in a cubic $Fd\bar{3}$. The unit cell is composed of eight symmetry equivalent hexaadducts placed in four unequal layers. Importantly, all the butylmalonate groups display an almost spherical arrange, with butyl

branches arranged in an all-stretched conformation (*A* conformation) as illustrated in Fig. 1 left. Similarly to **2**, the supramolecular packing is constructed through dihydrogen contacts (Fig. S2 and Table S2†).[11]

Physico-chemical study of polymorphs 2 and 3

The study of the thermal properties of both polymorphs was performed by thermogravimetric (TG) analysis and differential scanning calorimetry (DSC). Thermal stability studied by TG (see Fig. S3†) affords identical results for both **2** and **3**, with polymorphs not showing any loss of solvent between room temperature and 530 K, and irreversibly degrading for temperatures above. This experiment stablishes the degradation temperature limit to perform further physico-chemical studies to be 520 K.

Differential scanning calorimetry of polymorph **2** (Fig. 2 a) reveals two endothermic transformations at 387 K (single peak, 7.224 J g^{-1}), 460 K and 490 K (double peak, 33.761 J g^{-1}). The latter being consistent with the melting point of the compound. However, the cooling curve only displays one exothermic peak, at 388 K (18.820 J g^{-1}). Remarkably, in the second heating ramp the endothermic peak at 387 K was not evidenced, and only the two endothermic peaks at 460 K and 490 K (32.501 J g^{-1}) appear (see ESI† for further information). In the case of polymorph **3**, the heating thermogram only displays two endothermic peaks with similar values to those reported for **2**, *i.e.* 460 K and 490 K (33.761 J g^{-1}). The exothermic peaks recorded in the cooling process are similar to **2**. The thermal behaviour of both compounds shows a similar trend, as expected for polymorphs, the only difference being the endothermic peak observed for **2** at 387 K, which may be attributed to a phase transition.

Further insight into this phase transition was attained by monitoring single crystals of the polymorphs with an optical microscope equipped with a heating-and-cooling stage. The setup allows collecting the optical reflectivity of the sample

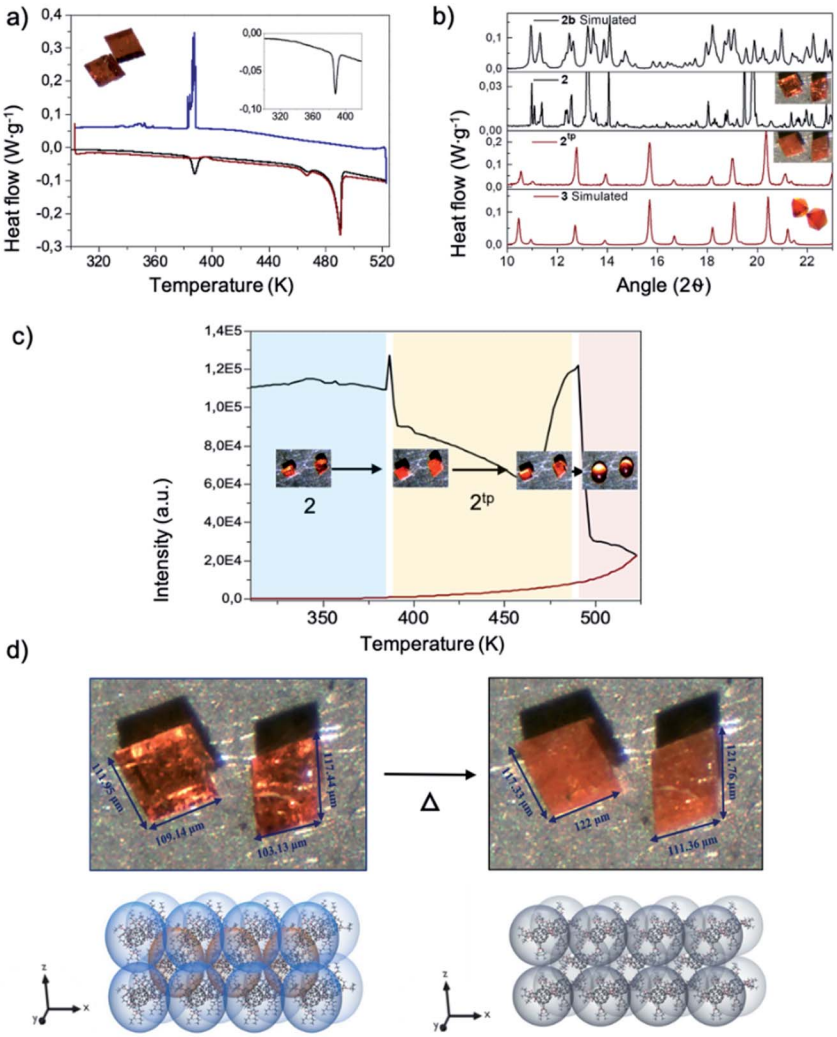

Fig. 2 (a) DSC curve as a function of temperature of **2** showing amplification of an endothermic peak at 387 K in the first heating ramp. (b) Simulated and experimental powder X-ray diffraction patterns of **2** and its simulated, phase transition compound $\mathbf{2}^{tp}$ and compound **3**. (c) Optical reflectivity as a function of temperature measurements of three consecutives heating and cooling ramps (d) Crystal size and shape variation at 298 K and after the phase transition at 387 K and a schematic illustration of the supramolecular rearrangement along the **2** to **3** transformation.

crystals while varying the temperature. To be consistent with the DSC measurements, similar thermals ramps were used. The reflectivity evolution against temperature for **2** is plotted in Fig. 2d and S6.† Similarly, to what is observed by DSC, **2** clearly shows two peaks at 387 K and 493 K. Close looks to the crystal images against temperature of the 387 K peak evidences a crystallinity variation and, more importantly, a noticeable crystal size change. The size of the crystal increases in the order of $\bar{x} =$ 5.25% (Fig. 2d and Video 1†). The 493 K peak undoubtedly corresponds to the fusion of **2**. In addition, it should be mentioned that the peaks of the cooling ramp and second heating ramp are not reflected in the optical reflectivity, the video recorded revealed what these peaks represent; the exothermic peak at 388 K indicated the recrystallization of the liquid form of **2** and the peak at 490 K again corresponds to the fusion of the compound.

Structural study of polymorph 2 after thermal treatment (2^{tp})

The lack of crystallinity of the new thermal phase obtained from **2** (namely 2^{tp}) prevented from solving the single-crystal diffraction pattern. However, in order to obtain more information about the nature of this new thermal phase, structural and physical studies, such as powder X-ray diffraction (PXRD) and FTIR were performed. Both experiments take advantage of the fact that the thermal phase transition leading to 2^{tp} is irreversible. PXRD were collected at room temperature and at 387 K and then compared with its simulated from their crystal structure by using Mercury software.[25] Both experimental and simulated PXRD spectra of **2** are almost superimposable as would be expected (see Fig. 2b). Then, **2** was heated for one hour at 375 K and 2^{tp} collected. The first observation is that the spectrum of 2^{tp} is different from **2**, which is in agreement with a phase transition behavior. In addition, a comparison between 2^{tp} and **3** diffractograms show an almost-perfect match. Thereby, 2^{tp} and **3** are the same compound.

Structurally the conversion from **2** to **3** is comprehensible. As aforementioned, compound **2** shows two different conformations where the arms are stretched out, bent and in an intermediate state. When applying temperature to **2**, the thermal transition leads to 2^{tp}.

In conclusion, when temperature is increased, all butyl branches go into a close-related stretched conformation, like reported for **3**. Importantly, as mentioned, the thermal transition from **2** to **3** is not reversible. However, polymorph **2** was regenerated from **3** by dissolving in an ethanol solution at 393 K for 3 days in the absence of metallic salt.

Hydrogenation of polymorph 2

Single-crystal to single-crystal reaction of polymorph **2** with hydrazine was studied. After 7 days of exposition of single crystals of **2** to hydrazine vapors at 67 °C, crystals remarkably change from orange to bright-yellow (see Fig. 3 and 4). This color change is indicative of the partial hydrogenation of **2** by hydrazine.[22] The resulting material attained by SCSC reaction, namely **2hyd**, agrees with the $C_{126}H_{132}O_{24}$ formulation, with twenty-four hydrogen atoms more than **2** ($C_{126}H_{108}O_{24}$). The

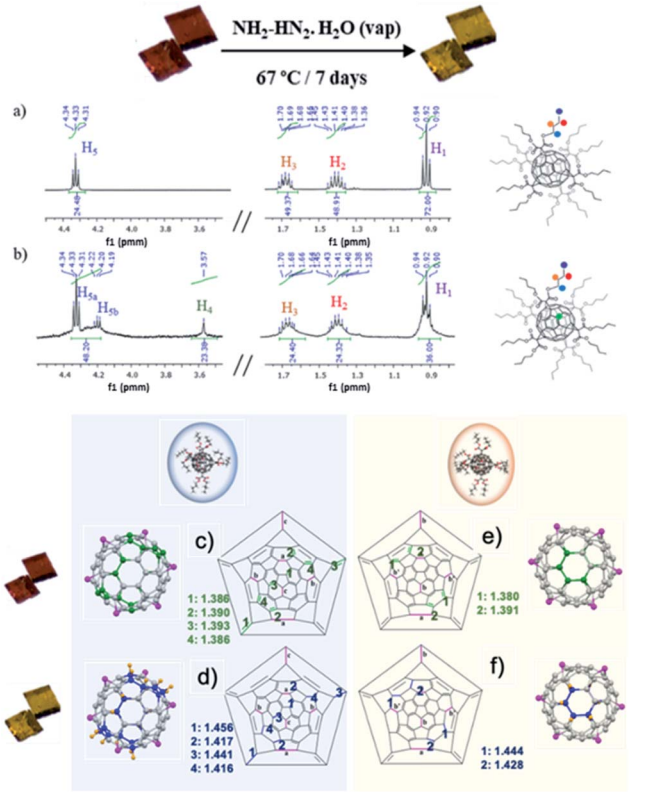

Fig. 3 Schematic view of 2hyd SCSC reaction by the exposition to hydrazine vapors and the ^{1}H NMR spectra of compounds (a) 2 and (b) 2hyd. Schlegel diagrams showing the comparison between distances before and after hydrogenation (c–f).

new material is stable under atmospheric conditions and highly soluble in common organic solvents such as CH_2Cl_2, CH_3Cl, and acetone. Additionally, the characterization of **2** and **2hyd** was carried out by standard spectroscopic techniques and was greatly facilitated by their high symmetry (see ESI† for full details).

The ^{1}H NMR spectra of **2** and **2hyd** are shown and described in Fig. 3, S9 and S10.† ^{1}H NMR spectrum of **2** displays four signals at 4.33, 1.68, 1.41 and 0.92 ppm which are consistent with twelve equivalent butyl malonates –OCH_2 (H5), –CH_2 (H3), –CH_2 (H2) and –CH_3 (H1), respectively (see Fig. 3a and b). The hydrogenation of **2** is evidenced in **2hyd** ^{1}H NMR spectrum by the emergence of a broad singlet at 3.57 ppm (–CH (H4)) integrating for 24H. A splitting of the 4.33 ppm triplet (–COOCH_2–) is also observed. Three well defined sets of signals are detected for these protons. As a result of the partial hydrogenation of the fullerene, each butyl chain of every malonate may fall into different magnetic environments. Every methylene lying above a non-hydrogenated hexagon remains at its original chemical shift, although two new multiplets arise between 4.30 and 4.20 ppm (see Fig. 3b), allegedly corresponding to methylenes placed above hydrogenated hexagons. In this regard, MS spectrum of **2hyd** confirms the presence of two molecular peaks at 2013.7 and 2021.8 *m*/*z* (see Fig. S12†), attributable to species gaining 8 and 16 protons, respectively.

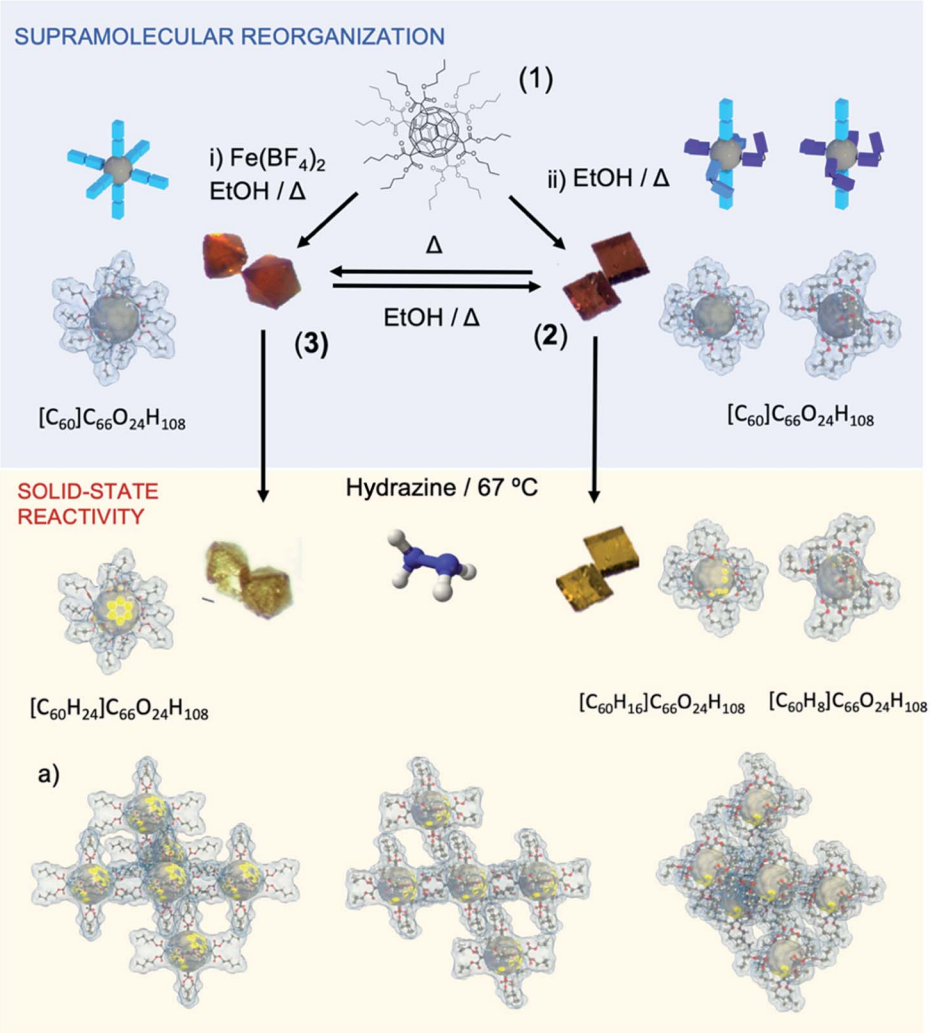

Fig. 4 Illustration summarizing the hexakis[60]fullerene supramolecular reorganization for **2** and **3** (blue on top) and the solid-state reactivity (hydrogenation with hydrazine under mild condition, in yellow). (a) Three simplified views of the 3D packing of the two polymorphs.

The hydrogenated compound **2hyd** is stable up to 423 K, when it starts decomposing according to thermogravimetric analysis, in contrast with its non-saturated precursor that decomposes just over 548 K (Fig. S3†). This stability loss is attributed to the increased strain supported by the fullerenes cage upon conversion of a large amount of sp^2 carbon atoms into sp^3. This is dramatically observed in the XRD crystal structure, where the cage seems to be rather bulgy than spherical.

Remarkably, the X-ray crystal structure of **2hyd** was solved (see Table S1† for further details), the hydrogenated material crystallizes in the triclinic space group $P\bar{1}$ as its precursor **2**, both showing a similar unit cell. A close look into the crystal structure indicates that the supramolecular reorganization between fullerene **2** and **2hyd** is almost the same, the crystal packing remaining unaffected after and before hydrogenation. This result has been reproduced several times, always obtaining the same consistent hydrogenation pattern. The hydrogenation of the fullerene is concomitant with a strong distortion of the buckyball caused by the acute pyramidalization (out of the plane buckyball process) of the carbons on hydrogenated hexagons as they shift from sp^2 hybridization to sp^3. This distortion is also exacerbated by the increase of their C–C bonding distances (see Fig. 3). Thus, by locating these bulges, the precise location of the hydrogenated carbons may be pointed (Fig. 3, 4 and S13†). With this aim, the different hydrogenation positions are plotted in the Schlegel diagram on Fig. 3c–f for the two different fullerene conformers present in the crystal structure. The pink colored linkages correspond to the cyclopropane rings attached to the butyl malonate groups, the green colored to the double linkages *prior* to the hydrogenation reaction, and the blue ones are the bond distances afterwards. From this representation, the precise position and distances involved during the hydrogenation, resulting in a change from sp^2 to sp^3 hybridization, may be found. In conclusion, crystallography data is in agreement with a partial hydrogenation of the crystals under hydrazine vapours, and the hydrogenation pattern of the hexaadducts of **2** is different

depending on the position they occupy in the unit cell due to the different conformation they adopt.

Thermal phase transition driving selective hydrogenation in fullerene-based materials. A confinement driven selective hydrogenation in solid–vapor reaction

As discussed above, the scaffold of **2** is composed by two distinct fullerenes, differentiated by the conformation adopted by their butyl malonate arms. Each fullerene experiences a dissimilar hydrogenation which may be owed to the different 3D disposition of the arms (Fig. 1 and S1†). For a better understanding, Fig. 4 shows a 3D representation correlating the different spatial conformations of the arms (*A*, *B* and *C*) with the buckyball bonds in which the hydrogenation occurs. From this representation, the dissimilar hydrogenation could be directly associated to the spatial disposition of the butyl malonate arms, which facilitates the hydrazine diffusion to the fullerene doble bonds and the subsequent formation of the reactive diimide species around the more stretched out arms (*A* and *B* conformations), allowing the hydrogenation of 8 double bonds (16H). In contrast, in fullerenes containing two additional pairs of bent arms, the steric hindrance of this contorted alkyl chains may obstruct the hydrazine diffusion, and consequently, only 4 double bonds result hydrogenated (8H). In the same direction, sample **3** has been examined and compared with **2**. Remarkably, **3** with 3 equal *A* conformations, shows a similar tendency as previously mentioned, *i.e.* **3** exclusively displays extended arms, thus favoring the access of hydrazine molecules to the buckyball and resulting in the hydrogenation of 12 double bonds (24H) of the fullerene hexaadduct.

Conclusion

We describe an unprecedented fullerene crystalline dynamic framework in compound **2** that exhibits an abrupt and irreversible phase transition in response to the temperature as external stimuli. This phase transition leads to the formation of a new polymorph, which by exhaustive characterization is found to be a crystalline material previously synthetized by our research group. By heating compound **2**, a complete stretching of the butyl arms (of both types of fullerenes present in **2**) occurs. This fact creates a densely compact 3D structure due to the reorganization of the butyl chains and their van der Waals contacts, as observed in the crystalline structure of $\mathbf{2^{tp}}$. In spite of not being a reversible phase transition, crystals of compound **2** can be obtained again by simple recrystallization (see Fig. 4). Finally, this thermal phase transition is also accompanied by a change of brightness and an expansion of the crystal size in the order of $\bar{x} = 5.25\%$. Thus, this experimental finding paves the way to be used in applications such as molecular actuators and machines. Exposure of **2** to hydrazine vapors induces color change from orange to yellow, which is indicative of the hydrogenation of the fullerenes composing the material.

The metal salt plays an active role in the supramolecular reorganization affording polymorph **3**. In parallel, the physicochemical and structural data acquired show unquestionably that the iron salt is not included in **3**. *e.g.*, the TGA curve shows no mass loss until decomposition of the organic fullerene (as reported in polymorph **2**) illustrating the absence of other molecules but purely the hexakisfullerene, not even traces of water molecules, that are usually part of these salts, as can be evidenced by FTIR. Unfortunately, the mechanism is not yet clear and further work are needed to clarify the role of salt.

It is noteworthy to mention that the hydrogenation of alkenes and dienes is critical in academia and industry (pharmaceuticals, petrochemicals, fine chemical synthesis).[26] Although this reaction is well described, *e.g.* Lindlar catalysts,[27] the symmetrical diene hydrogenation remains limited due mainly by a lack in the selectivity (both regio- and chemoselectivity).[28] In this work, the control in the supramolecular rearrangement is used to selectively hydrogenate hexakisfullerenes in a metal-free manner. In fact, a different hydrogenation pattern of the fullerenes is observed depending on the place they occupy at the unit cell of the crystal. Fullerenes bearing more butylmalonate groups with less contorted conformations (*A* and *C*) receive up to 16 hydrogens, whereas the ones bearing more groups in contorted conformations (*B*) just receive 8 hydrogens. The relative spatial disposition of the butyl malonate arms is essential for the diimide generation reaction taking place over reactive double bond sites.[29] These controlled solid-state reactions will contribute to the creation of novel soft and dynamic carbon-based advanced absorbent materials with a variety of direct technological applications, as chemosensors and environmental remediation devices. In addition, once the scaling process limitation could be addressed, these polymorphs could play an important role in the synthesis of new fullerene derivatives.

Author contributions

The work was conceived and directed by JSC and NM. EFB, AG, JS, SK, ERS performed sample preparation and chemical analysis. EFB, AG, JS, analyzed the data. EFB and ECS collected the single crystal X-ray diffraction and ECS solved the structures. EFB, AG, JS and JSC wrote the paper, and all authors discussed the experimental results.

Conflicts of interest

There are no conflicts to declare.

Acknowledgements

JSC is grateful to the Spanish MINECO for financial support through National Research Project (PID2019-111479GB-I00) and the Ramon y Cajal Research program (RYC-2014-16866) for funding support. IMDEA Nanociencia acknowledges support from the 'Severo Ochoa' Programme for Centres of Excellence in R&D (MINECO, Grant SEV-2016-0686). ECS acknowledges financial support from the Spanish Government, (Grant CTQ2015-68370-P). JS, ERS and NM thank the MINECO of Spain (Project CTQ2017-83531-R). We would like to thank to XALOC-ALBA synchrotron source under the project no. (2018012561).

Notes and references

1 J.-M. Lehn, *Angew. Chem., Int. Ed.*, 2015, **54**, 3276–3289.
2 J.-M. Lehn, *Chem. Soc. Rev.*, 2017, **46**, 2378–2379.
3 H. Yamagishi, H. Sato, A. Hori, Y. Sato, R. Matsuda, K. Kato and T. Aida, *Science*, 2018, **361**, 1242–1246.
4 D. Van Craen, W. H. Rath, M. Huth, L. Kemp, C. Räuber, J. M. Wollschläger, C. A. Schalley, A. Valkonen, K. Rissanen and M. Albrecht, *J. Am. Chem. Soc.*, 2017, **139**, 16959–16966.
5 M. Wehner, M. Insa Silja Röhr, V. Stepanenko and F. Würthner, *Nat. Commun.*, 2020, **11**, 5460.
6 W. S. Horne and T. N. Grossmann, *Nat. Chem.*, 2020, **12**, 331–337.
7 D. D. Prabhu, K. Aratsu, Y. Kitamoto, H. Ouchi, T. Ohba, M. J. Hollamby, N. Shimizu, H. Takagi, R. Haruki, S. Adachi and S. Yagai, *Sci. Adv.*, 2018, **4**, eaat8466.
8 O. Sato, *Nat. Chem.*, 2016, **8**, 644–656.
9 K. Biradha and R. Santra, *Chem. Soc. Rev.*, 2013, **42**, 950–967.
10 J.-H. Deng, J. Luo, Y.-L. Mao, S. Lai, Y.-N. Gong, D.-C. Zhong and T.-B. Lu, *Sci. Adv.*, 2020, **6**, eaax9976.
11 J. Echeverría, G. Aullón, D. Danovich, S. Shaik and S. Alvarez, *Nat. Chem.*, 2011, **3**, 323–330.
12 D. M. Guldi, B. M. Illescas, C. M. Atienza, M. Wielopolski and N. Martín, *Chem. Soc. Rev.*, 2009, **38**, 1587.
13 A. Muñoz, D. Sigwalt, B. M. Illescas, J. Luczkowiak, L. Rodríguez-Pérez, I. Nierengarten, M. Holler, J.-S. Remy, K. Buffet, S. P. Vincent, J. Rojo, R. Delgado, J.-F. Nierengarten and N. Martín, *Nat. Chem.*, 2016, **8**, 50–57.
14 A. Kraft, P. Roth, D. Schmidt, J. Stangl, K. Müller-Buschbaum and F. Beuerle, *Chem. –Eur. J.*, 2016, **22**, 5982–5987.
15 A. M. Rice, E. A. Dolgopolova and N. B. Shustova, *Chem. Mater.*, 2017, **29**, 7054–7061.
16 P. Peng, F.-F. Li, V. S. P. K. Neti, A. J. Metta-Magana and L. Echegoyen, *Angew. Chem., Int. Ed.*, 2014, **53**, 160–163.
17 P. Peng, F.-F. Li, F. L. Bowles, V. S. P. K. Neti, A. J. Metta-Magana, M. M. Olmstead, A. L. Balch and L. Echegoyen, *Chem. Commun.*, 2013, **49**, 3209.
18 N. K. Minar, K. Hou, C. Westermeier, M. Döblinger, J. Schuster, F. C. Hanusch, B. Nickel, G. A. Ozin and T. Bein, *Angew. Chem., Int. Ed.*, 2015, **54**, 7577–7581.
19 A. Kraft and F. Beuerle, *Tetrahedron Lett.*, 2016, **57**, 4651–4663.
20 D. E. Williams, E. A. Dolgopolova, D. C. Godfrey, E. D. Ermolaeva, P. J. Pellechia, A. B. Greytak, M. D. Smith, S. M. Avdoshenko, A. A. Popov and N. B. Shustova, *Angew. Chem., Int. Ed.*, 2016, **55**, 9070–9074.
21 A. Kraft, C. Roger, D. Schmidt, J. Stangl, K. Müller-Buschbaum and F. Beuerle, *Chem. –Eur. J.*, 2017, **23**, 15864–15868.
22 E. Fernandez-Bartolome, J. Santos, A. Gamonal, S. Khodabakhshi, L. J. McCormick, S. J. Teat, E. C. Sañudo, J. S. Costa and N. Martín, *Angew. Chem., Int. Ed.*, 2019, 28–31.
23 I. Lamparth, C. Maichle–Mössmer and A. Hirsch, *Angew. Chem., Int. Ed. Engl.*, 1995, **34**, 1607–1609.
24 M. V. Korobov, A. L. Mirakian, N. V. Avramenko, E. F. Valeev, I. S. Neretin, Y. L. Slovokhotov, A. L. Smith, G. Olofsson and R. S. Ruoff, *J. Phys. Chem. B*, 1998, **102**, 3712–3717.
25 O. V. Dolomanov, L. J. Bourhis, R. J. Gildea, J. A. K. Howard and H. Puschmann, *J. Appl. Crystallogr.*, 2009, **42**, 339–341.
26 M. Miyazaki, S. Furukawa and T. Komatsu, *J. Am. Chem. Soc.*, 2017, **139**, 18231–18239.
27 H. Lindlar, *Helv. Chim. Acta*, 1952, **35**, 446–450.
28 X. Zhang, H. Shi and B.-Q. Xu, *Angew. Chem., Int. Ed.*, 2005, **44**, 7132–7135.
29 A. Dhakshinamoorthy, J. He, A. Franconetti, A. M. Asiri, A. Primo and H. Garcia, *Catal. Sci. Technol.*, 2018, **8**, 1589–1598.